**Subtropical marine low stratiform cloud deck spatial errors in the E3SMv1 Atmosphere Model**

Michael A. Brunke[1], Po-Lun Ma[2], J. E. Jack Reeves Eyre[1], Philip J. Rasch[2], Armin Sorooshian[1,3], and Xubin Zeng[1]

[1]Department of Hydrology and Atmospheric Sciences, The University of Arizona, Tucson, AZ
[2]Pacific Northwest National Laboratory, Richland, WA
[3]Department of Chemical and Environmental Engineering, The University of Arizona, Tucson, AZ

## Contents of this file

## Introduction

The text, table, and figures presented here are auxiliary information for the main text. The same data processed as in the main text are used in these supplemental figures.

## S1  Description of the model physics and uncertainties in COSP

The previous version 0 of the E3SM is a descendent of CESM1. The atmospheric component of the current version 1, the E3SM Atmosphere Model version 1 (EAMv1), uses a spectral element dynamical core at standard low (~100 km) and high (~25 km) horizontal resolutions, and adopts a much higher vertical resolution. The primary changes in EAMv1 physics relevant to this study include the use of Cloud Layers Unified by Binormals (CLUBB, Bogenschutz et al., 2012; Golaz et al., 2002; Larson et al., 2002; Larson and Golaz, 2005; Larson, 2017) for turbulence, shallow convection, and cloud macrophysics; the second version of Morrison and Gettelman microphysics (MG2, Gettelman and Morrison, 2015); and the 4-mode version of the Modal Aerosol Module

(MAM4) with marine organics (Burrows et al., 2016). The general characteristics of clouds and precipitation are documented in Xie et al. (2018).

CAM5's moist turbulence is characterized by the Bretherton and Park (2009) parameterization, while microphysics is represented by the older MG1 (Morrison and Gettelman, 2008). Stratiform condensation and cloud fraction are similar to Zhang et al. (2003) as adapted in Neale et al. (2010). CM3's stratiform cloud liquid and fraction are determined according to Tiedtke (1993) as adapted by Anderson et al. (2004) and Donner et al. (2011). Shallow cumulus is parameterized as in Bretherton et al. (2004). Subgrid variability is allowed by considering a normally-distributed vertical velocity with cloud droplet activation determined through integration (Ghan et al., 1997).

In ModelE2, stratiform cloud water is determined prognostically by a Sundqvist-type scheme with cloud fraction determined diagnostically (Del Genio et al., 1996). Updates to this scheme from ModelE were explained in Schmidt et al. (2006).

Further details on the above CMIP5 models can be found in Meehl et al. (2013) for CAM5, Donner et al. (2011) for CM3, and Schmidt et al. (2014) for ModelE2.

In this study, we use the LCC from the CALIPSO satellite simulator in the models, but Song et al. (2018) found a discrepancy between satellite simulator cloud fraction and model diagnostic cloud fraction due to deficiencies in the sub-column generator in COSP. We compare the model diagnostic LCCs from the E3SMv1 runs to those from the satellite simulator in Fig. S8. Generally, the one-to-one line lies within the bulk of the 25th and 75th percentiles of binned diagnostic LCCs. The model diagnostic values can be much higher than COSP values as represented by the maximum bin diagnostic LCCs, but this is particularly problematic for low LCCs from the satellite simulator, consistent with Song et al. (2018). This problem is reduced for LCC > ~40% which is a focus of this paper, because the diagnostic clouds are likely to be more homogeneous for these LCCs. Therefore, we continue to rely on the satellite simulator LCCs, but we use multiple observational datasets in model evaluations (see Section 2.2).

## S2  Other satellite climatologies used in this study

To better quantify the uncertainty in using other climatologies from previous studies, we also utilize data from the International Satellite Cloud Climatology Project (ISCCP) D2 product. In these products, the various cloud types are differentiated by cloud top pressure and cloud optical thickness. D2 is the climatological summary product that provides monthly mean CF for each layer (low, middle, and high) and for each individual type using the revised algorithm (Rossow and Schiffer, 1999) on a 280-km equal area grid. The D2 CFs are regridded to a 2.5° × 2.5° regular grid.

Furthermore, we compare the two satellite CF products to in-situ global observations from an update to the Warren et al. (1986, 1988) climatology, the Extended Edited Cloud Reports Archive (EECRA, Hahn and Warren, 2009; Eastman et al., 2011). This climatology provides seasonal mean CF for the various layers (low, middle,

and high) as well as the various cloud types in each layer on a 5° × 5° equal-area regular grid.  We use the ocean climatology for 1954-1997.

**S3  Defining the LCC45+ decks**

Since low-level stratiform clouds can co-exist with other cloud types including cumuliform clouds, a threshold should be chosen to differentiate a regime in which low stratiform clouds (that we are most interested in) are dominant versus those for lower LCC in which they are not necessarily so.  The median frequency of low stratiform clouds in the 2B-CLDCLASS-LIDAR product in all of the extended regions rises above ~40% for LCC > 50% CF, whereas high and middle cloud frequencies decrease below ~40% for LCC > 30% CF (Figure S9).  Shallow cumulus clouds are less frequent than both of these cloud types for all LCCs.  Thus, low stratiform clouds are increasingly dominant for LCC > 40% CF.  Therefore, we choose an LCC threshold of 45% CF to define the stratiform cloud decks.  We call these regions the LCC45+ decks.

**S4  Evaluation of the E3SMv1 coupled historical simulation**

Additional dynamical sensitivity can be studied when coupling the atmosphere model to an ocean model.  The sensitivity of this coupling can be assessed by comparing the results from the fully coupled historical simulations versus the prescribed SST AMIP runs.  The ensemble mean of the former generally produces similar mean annual cycles in LCC to that of the latter in all of the LCC45+ decks.  Notably in the NEP, the coupled historical runs do not produce a maximum in July as in the AMIP runs, decreasing from May until September (Figure 1).  During this decreasing LCC period, historical LCC is 4% CF lower than that of the AMIP runs.  Some improvement is found for some seasons and decks in centroid distances, while area and overlap ratios generally are reduced (Figure 2).  Average centroid distances over all seasons for the historical ensemble mean range from 54 to 1316 km compared to 88-995 km in the AMIP runs.  Average area ratios for the historical ensemble are 0.21-1.16 (which are better compared to 0.78-1.08 in the AMIP runs), and average overlap ratios are 0.20-0.81 (which are worse compared to 0.16-0.63 in AMIP).

**References**

Anderson, J.L., Balaji, V., Broccoli, A.J., Cooke, W.F., Delworth, T.L., Dixon, K.W., et al. (2004).  The new GFDL global atmosphere and land model AM2-LM2:  Evaluation with prescribed SST simulations. *Journal of Climate*, *17*, 4641-4673.

Bogenschutz, P.A., Gettelman, A., Morrison, H., Larson, V.E., Schanen, D.P., Meyer, N.R., Craig, C. (2010).  Unified parameterization of the planetary boundary layer and shallow convection with a higher-order turbulence closure in the Community Atmosphere Model:  single-column experiments. *Geoscientific Model Development*, *5*, 1407-1423.  https://doi.org/10.5194/gmd-5-1407-2012.

Bretherton, C.S., Park, S. (2009). A new moist turbulence parameterization in the Community Atmosphere Model. *Journal of Climate*, *22*, :3422-3448. https://doi.org/10.1175/2008JCLI2556.1

Bretherton, C.S., McCaa, J.R., Grenier, H. (2004). A new parameterization for shallow cumulus convection and its application to marine subtropical cloud-topped boundary layers. Part I: Description and 1D results. *Monthly Weather Review*, *132*, 864-882.

Burrows, S.M., Gobrogge, E.A., Fu, L., Link, K.A., Elliott, S., Wang, H., Walker, R.A. (2016). OCEANFILMS-2: Representing coadsorption of saccharides in marine films and potential impacts on modeled marine aerosol chemistry. *Geophysical Research Letters*, *43*, 8306-8313. https://doi.org/10.1002/2016GL069070.

Del Genio, A.D., Yao, M.-S., Kovari, W., Lo, K.-W. (1996). A prognostic cloud water parameterization for global climate models. *Journal of Climate*, *9*, 270-304. https://doi.org/10.1175/1520-0442(1996)009<0270:APCWPF>2.0.CO;2.

Donner, L.J., Wyman, B.L., Hemler, R.S., Horowitz, L.W., Ming, Y., Zhao, M., et al. (2011). The dynamical core, physical parameterizations, and basic simulation characteristics of the atmospheric component AM3 of the GFDL global coupled model CM3. *Journal of Climate*, *24*, 3484-3519. https://doi.org/10.1175/2011JCLI3955.1.

Eastman, R., Warren, S.G., Hahn, C.J. (2011). Variations in cloud cover and cloud types over the ocean from surface observations, 1954-2008. *Journal of Climate*, *24*, 5914-5934. https://doi.org/10.1175/2011JCLI39772.1.

Gettelman, A., Morrison, H. (2015). Advanced two-moment bulk microphysics for global models. Part I: Off-line tests and comparison with other schemes. *Journal of Climate*, *28*, 1268-1287. https://doi.org/10.1175/JCLI-D-14-00102.1.

Ghan, S.J., Leung, L.R., Easter, R.C., Abdul-Razzak, H. (1997). Prediction of cloud droplet number in a general circulation model. *Journal of Geophysical Research*, *102*, 21 777-21 794.

Golaz, J.-C., Larson, V.E., Cotton, W.R. (2002). A PDF-based model for boundary layer clouds. Part I: Method and model description. *Journal of the Atmospheric Sciences*, *59*, 3540-3551.

Hahn, C.J., Warren, S.G. (2009). Extended edited synoptic cloud reports from ships and land stations over the globe, 1952-1996 (2009 update) (CDIAC Numerical Data Package NDP-026C). Oak Ridge, TN: Carbon Dioxide Information Analysis Center, Oak Ridge National Laboratory. https://doi.org/10.3334/CDIAC/cli.ndp026c.

Larson, V.E. (2017). *CLUBB-SILHS: A parameterization of subgrid variability in the atmosphere* (ArXIV:1711.03675 [Physics]). http://arxiv.org/abs/1711.03675.

Larson, V.E., Golaz, J.-C. (2005). Using probability density functions to derive consistent closure relationships among higher-order moments. *Monthly Weather Review*, *133*, 1023-1042. https://doi.org/10.1175/MWR2902.1

Larson, V.E., Golaz, J.-C., Cotton, W.R. (2002). Small-scale and mesoscale variability in cloudy boundary layers: Joint probability density functions. *Journal of the Atmospheric Sciences*, *59*, 3519-3539. https://doi.org/10.1175/1520-0469(2002)059<3519:SSAMVI>2.0.CO;2.

Meehl, G.A., Washington, W.M., Arblaster, J.M., Hu, A., Teng, H., Kay, J.E., Gettelman, A., Lawrence, D.M., Sanderson, B.M., Strand, W.G. (2013). Climate change projections in CESM1(CAM5) compared to CCSM4. *Journal of Climate*, *26*, 6287-6308. https://doi.org/10.1175/JCLI-D-12-00572.1.

Morrison, H., Gettelman, A. (2008). A new two-moment bulk stratiform cloud microphysics scheme in the NCAR Community Atmosphere Model (CAM3), Part I: Description and numerical tests. *Journal of Climate*, *21*, 3642-3659. https://doi.org/10.1175/2008JCLI2105.1.

Neale, R.B., Chen, C.-C., Gettelman, A., Lauritzen, P.H., Park, S., Williamson, D.L., et al. (2010). *Description of the NCAR Community Atmosphere Model (CAM 5.0)* (NCAR Tech. Note NCAR/TN-486+STR). Boulder, CO: National Center for Atmospheric Research.

Rossow, W.B., Schiffer, R.A. (1999). Advances in understand clouds from ISCCP. *Bulletin of the American Meteorological Society*, *80*, 2261-2287.

Schmidt, G.A., Kelley, M., Nazarenko, L., Ruedy, R., Russell, G.L., Aleinov, I., et al. (2014). Configuration and assessment of the GISS ModelE2 contributions to the CMIP5 archive. *Journal of Advances in Modeling Earth Systems*, *6*, 141-184. https://doi.org/10.1002/2013MS000265.

Schmidt, G. A., Ruedy, R., Hansen, J. E., Aleinov, I., Bell, N., Bauer, M., et al. (2006). Present-day atmospheric simulations using GISS ModelE: Comparison to in situ, satellite, and reanalysis data. *Journal of Climate*, *19*, 153-192.

Song, H., Zhang, Z., Ma, P.-L., Ghan, S., Wang, M. (2018). The importance of considering sub-grid cloud variability when using satellite obserations to evaluate the cloud and precipitation simulations in cloud models. *Geoscientific Model Development*, *11*, 3147-3158. https://doi.org/10.5194/gmd-11-3147-2018.

Tiedtke, M. (1993). Representation of clouds in large-scale models. *Monthly Weather Review*, *121*, 3040-3061.

Warren, S.G., Hahn, C.J., London, J., Chervin, R.M., Jenne, R.L. (1986). *Global distribution of total cloud cover and cloud type amounts over land* (NCAR Tech. Note TN-273+STR). Boulder, CO: National Center for Atmospheric Research.

Warren, S.G., Hahn, C.J., London, J., Chervin, R.M., Jenne, R.L. (1988). *Global distribution of total cloud cover and cloud type amounts over the ocean* (NCAR

Tech. Note TN-317+STR).  Boulder, CO:  National Center for Atmospheric Research.

Xie, S., Lin, W., Rasch, P.J., Ma, P.-L., Neale, R., Larson, V.E., Qian, Y., Bogenschutz, P.A., Caldwell, P., Cameron-Smith, P., Golaz, J.-C., Mahajan, S., Singh, B., Tang, Q., Wang, H., Yoon, J.-H., Zhang, K., Zhang, Y. (2018).  Understanding cloud and convective characteristics in version 1 of the E3SM Atmosphere Model. *Journal of Advances in Modeling Earth Systems*, *10*, 2618-2644. https://doi.org/10.1029/2018MS001350.

Zhang, M., Lin, W., Bretherton, C.S., Hack, J.J., Rasch, P.J. (2003).  A modified formulation of fractional stratiform condensation rate in the NCAR Communty Atmosphere Model (CAM2). *Journal of Geophysical Research-Atmospheres*, *108*, 4035.  https://doi.org/10.1029/2002JD002523.

**Table S1.** The Marine Subtropical Stratocumulus Regions.

| Marine subtropical stratiform cloud deck region | Core regions | Extended regions[a] |
|---|---|---|
| Northeast Pacific (NEP) | 20°-30°N, 120°-130°W | 10°-40°N, 110°-145°W |
| Northeast Atlantic (NEA) | 15°-25°N, 25°-35°W | 0°-30°N, 15°-50°W |
| Southeast Pacific (SEP) | 10°-20°S, 80°-90°W | 5°-35°S, 70°-105°W |
| Southeast Atlantic (SEA) | 10°-20°S, 0°-10°E | 5°-35°S, 20°W-15°E |
| Southern Indian Ocean (SIO) | 25°-35°S, 95°-105°E | 10°-40°S, 80°-115°E |

[a]LCC > 45% within these regions encapsulate all or most of the low stratiform cloud decks.
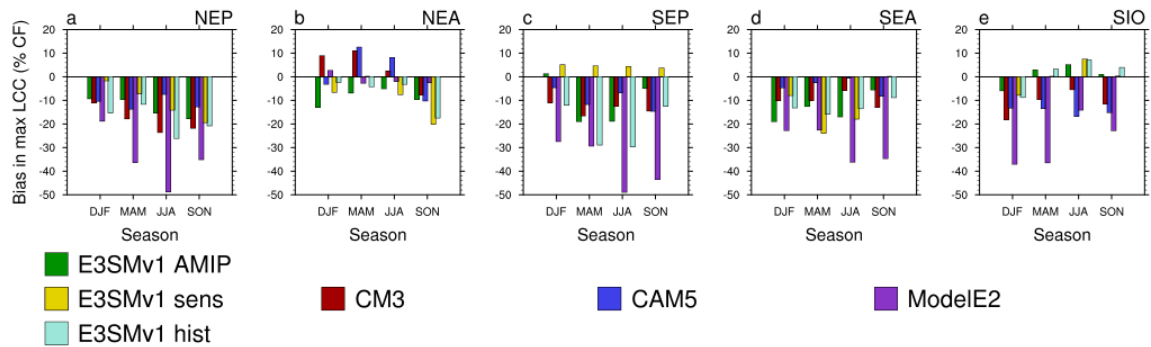


**Figure S1.** The biases in maximum low cloud cover (LCC) of the LCC45+ decks in E3SMv1 AMIP runs, CESM1-CAM5, GFDL CM3, GISS ModelE2, E3SMv1 sensitivity test, and E3SMv1 historical runs to GOCCP in each season and each region. No bar is shown whenever an LCC45+ deck is not produced by a model.
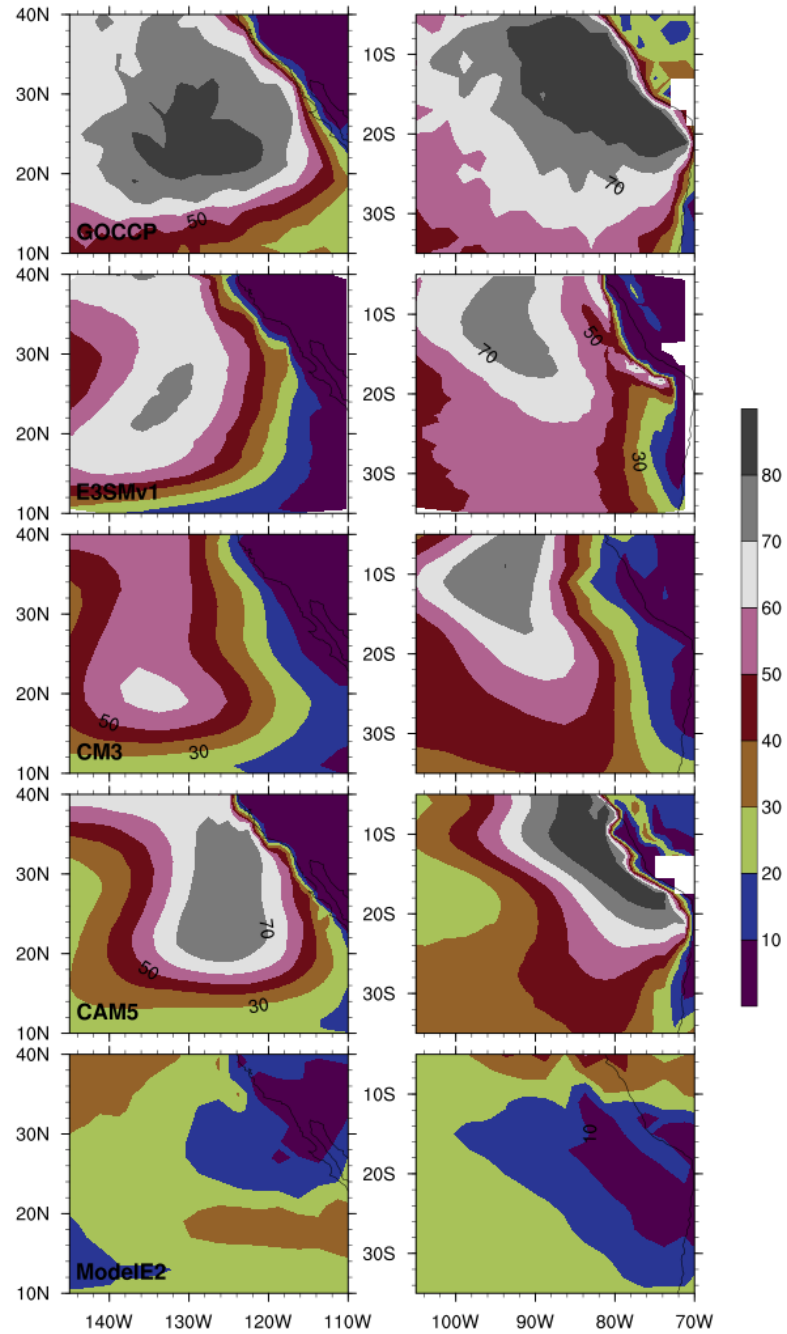
**Figure S2.** Seasonal mean LCC (% CF) in (left) NEP and (right) SEP in June-August (JJA) from (top to bottom) CALIPSO-GOCCP for 2007-2014, E3SMv1 for 1990-2009, GFDL CM3 for 1990-2008, CESM1-CAM5 for 1990-2005, and GISS ModelE2 for 1990-2009.
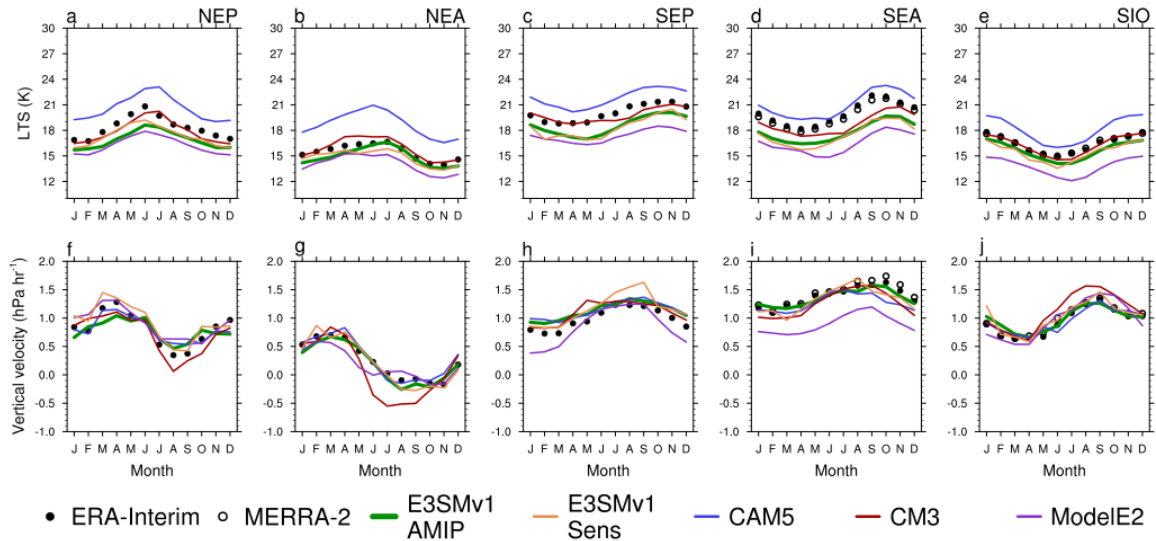
**Figure S3.** The mean annual cycle in lower tropospheric stability (LTS, top) and vertical velocity (bottom) from ERA-Interim and MERRA-2 versus E3SMv1, CESM1-CAM5, GFDL CM3, and GISS ModelE2 in the extended regions. The reanalyses, E3SMv1, and CESM1-CAM5 values were regridded to the coarser (2° latitude × 2.5° longitude) resolution of CM3 and ModelE2 before averaging.
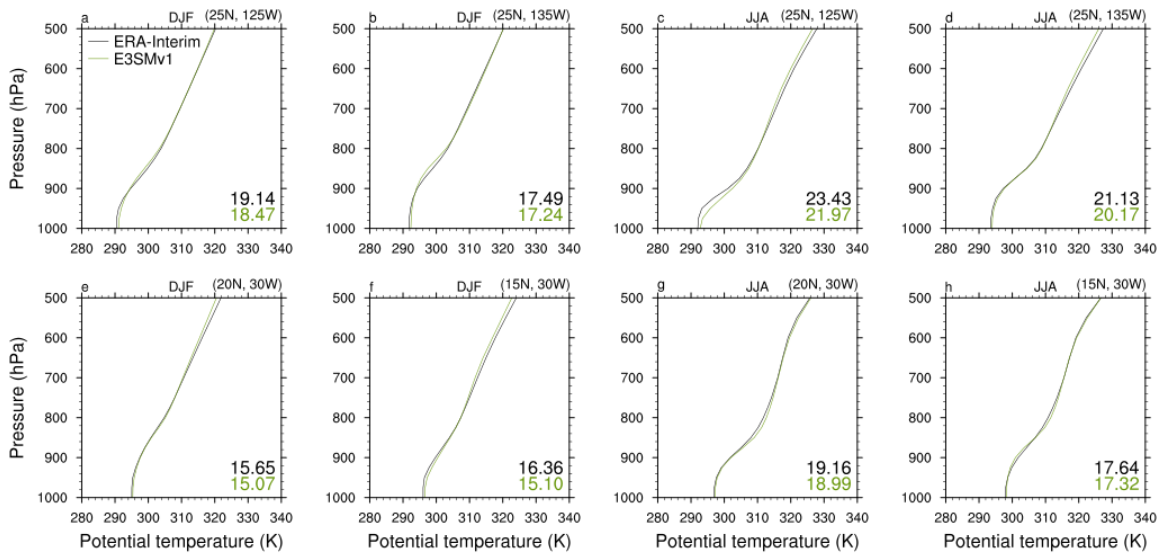


**Figure S4.** The potential temperature profiles up to 500 hPa in December-February (DJF) and June-August (JJA) in ERA-Interim (black) and E3SMv1 (green). Profiles are shown for grid cells in the middle of the core regions and farther offshore corresponding roughly to the center of the misplaced cloud decks in E3SMv1 in the (top) NEP and (bottom) SEP. The numbers in the bottom right are the lower tropospheric stability (LTS).

9
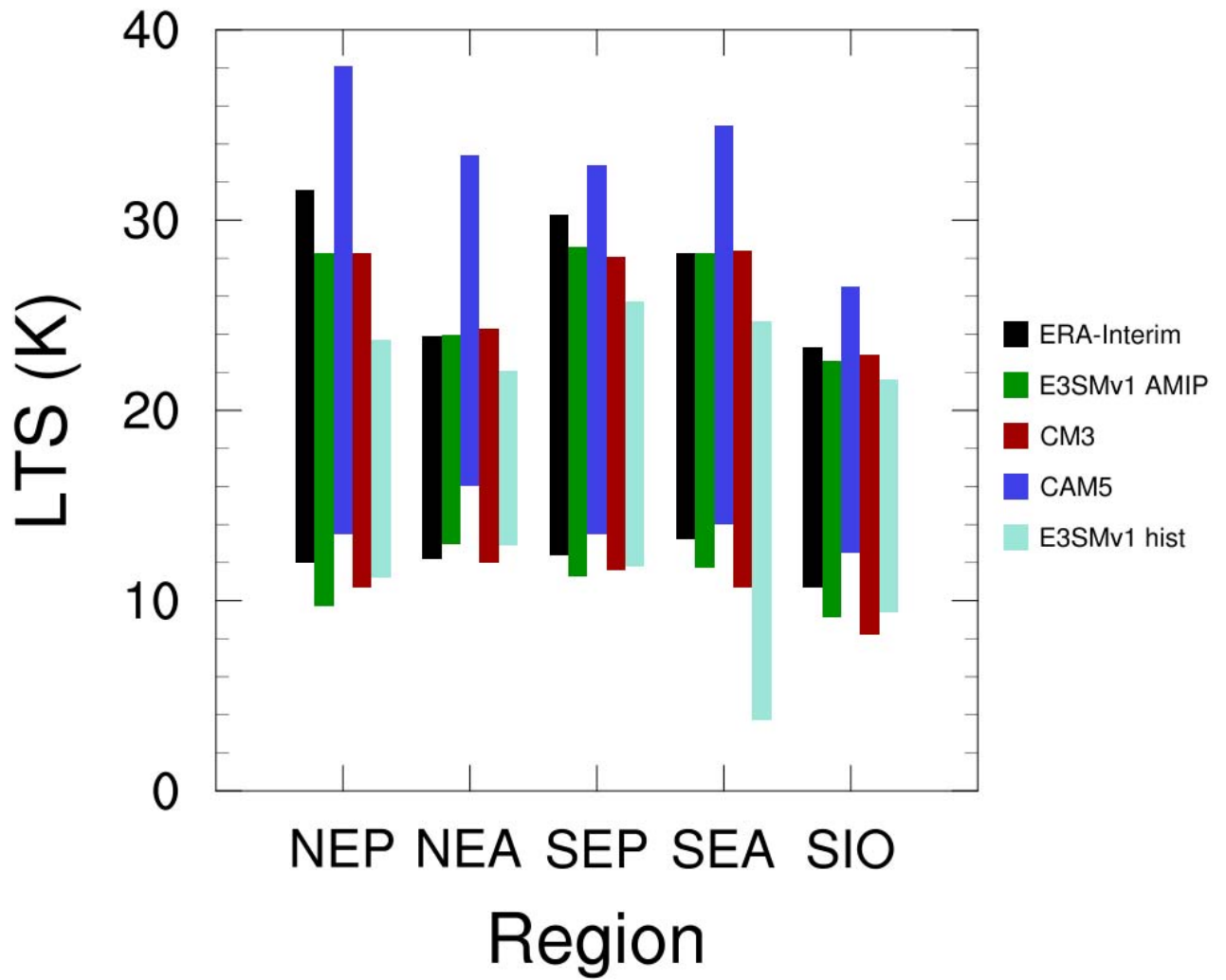
**Figure S5.** The range of LTS values in the LCC45+ decks in all months for each region in ERA-Interim, E3SMv1, GFDL CM3, and CESM1-CAM5.
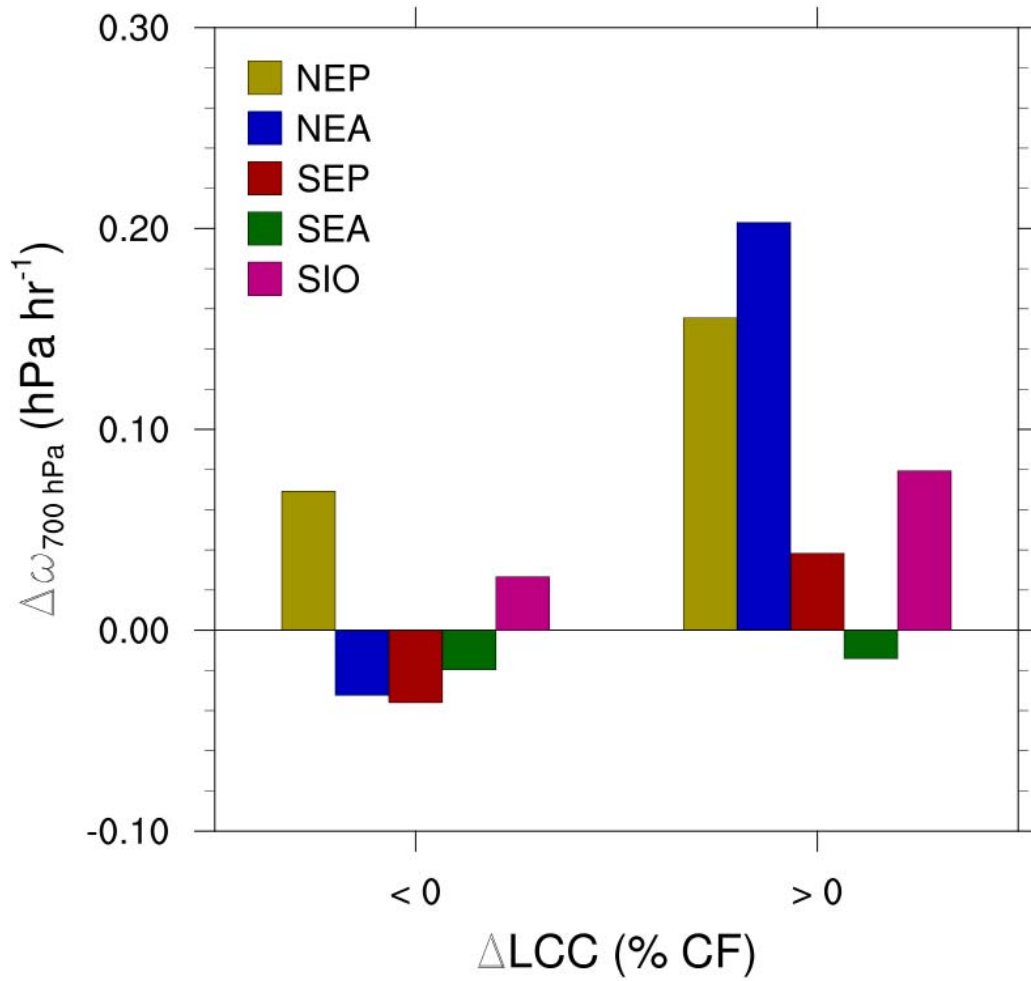
**Figure S6.** Median differences in 700-hPa vertical velocity ($\Delta\omega_{700\ hPa}$) for grid cells in which LCC is decreased ($\Delta$LCC < 0) and increased ($\Delta$LCC > 0) in each extended region.
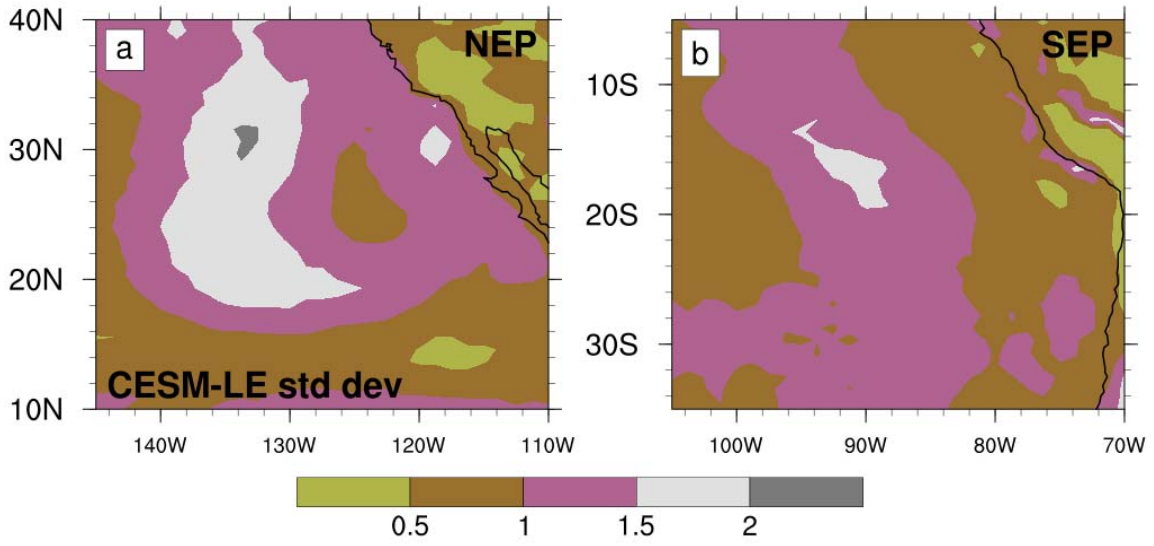
**Figure S7.** CESM large ensemble (CESM-LE) standard deviation in JJA seasonal mean LCC (% CF) in (a) NEP and (b) SEP. Note the difference in scale from Figure 3c-f.
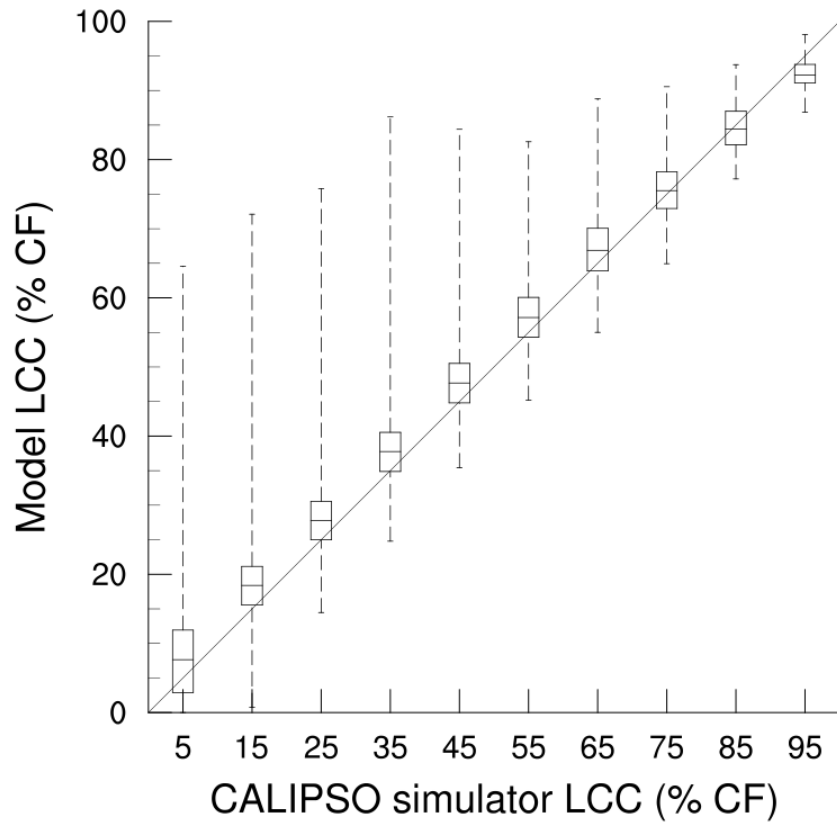
**Figure S8.** Boxplots of model-derived LCC for 10% CALIPSO simulator LCC bins from COSP over all of the extended regions in E3SMv1. The top and bottom of the boxes are the upper and lower quartiles, respectively, and the horizontal line indicates the bin medians. The wings of each box indicate the maximum and minimum values in the bin. The slantwise line represents the one-to-one line.
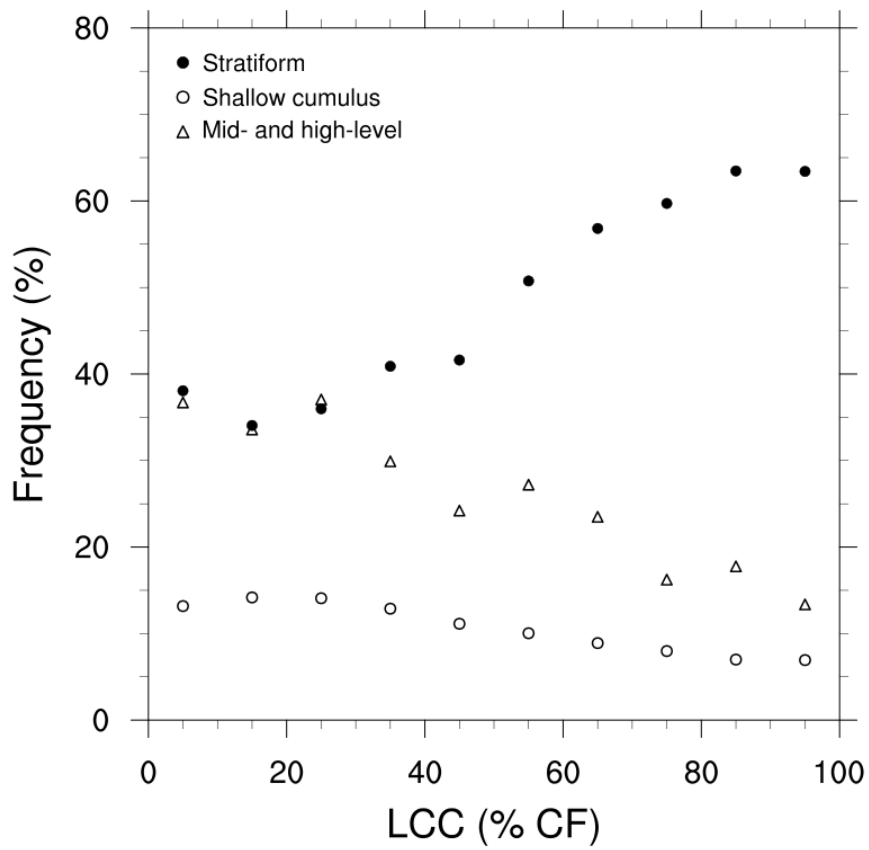
**Figure S9.** The median frequency of 2B-CLDCLASS-LIDAR cloud types per 10% CF bins of LCC in CALIPSO-GOCCP over all of the extended regions.